



Energy efficiency and stability of electric vehicles utilising direct yaw moment control

Peikun Sun ^{a,b}, Annika Stensson Trigell^{b,c}, Lars Drugge ^{b,c} and Jenny Jerrelind^{b,c}

^aDepartment of Military Trade Civil Radar, The 38th Institute of China Electronics Technology Group Corporation, Hefei, People's Republic of China; ^bKTH Vehicle Dynamics, Department of Engineering Mechanics, KTH Royal Institute of Technology, Stockholm, Sweden; ^cCentre for ECO2 Vehicle Design, KTH Royal Institute of Technology, Stockholm, Sweden

ABSTRACT

A direct yaw moment control (DYC) for energy-efficiency and a DYC for stability of electric vehicles (EVs) are proposed. The DYC for energy-efficiency is active during non-safety-critical cornering manoeuvres to improve the energy-efficiency of EVs. The DYC for stability is active during safety-critical manoeuvres to keep the vehicle stable. A combination of the DYC for energy-efficiency and the DYC for stability is studied. A stability judgement based on the yaw rate and slip angle is designed for evaluating the criticality of the vehicle's working state. A switching principle for alternating between the DYC for energy-efficiency and the DYC for stability is designed. During non-safety-critical cornering manoeuvres, it is shown that the DYC for energy efficiency can save considerable percentage of energy compared to both equal torque driving and the DYC for stability. During cornering manoeuvres containing both non-safety-critical parts and safety-critical parts, the simulation results in this work show that the combination of the DYC for energy-efficiency and the DYC for stability can give 12% to 18% energy savings compared to the DYC for stability only for the vehicle and manoeuvres studied.

ARTICLE HISTORY

Received 30 October 2019
Revised 29 August 2020
Accepted 16 October 2020

KEYWORDS

Electric vehicle;
energy-efficiency; direct yaw
moment control; stability

Nomenclature

β	Body slip angle
δ_f	Steering angle for the front wheels
κ_i	Slip ratio ($i = 1$: front left; $i = 2$: front right; $i = 3$: rear left; $i = 4$: rear right.)
μ	Road friction
ω_i	Wheel angular velocity ($i = 1, 2, 3, 4$)
ψ	Yaw angle
A	Frontal area of the vehicle
a_y	Lateral acceleration
C_f	Front cornering stiffness
C_r	Rear cornering stiffness

CONTACT Peikun Sun  peikun@kth.se

f_{rr}	Rolling resistance coefficient
F_{xi}	Longitudinal force ($i = 1, 2, 3, 4$)
F_{yi}	Lateral force ($i = 1, 2, 3, 4$)
F_{zi}	Vertical force ($i = 1, 2, 3, 4$)
I_z	Moment of yaw inertia
l_f	Distance from CoG to front axle
l_r	Distance from CoG to rear axle
m	Vehicle mass
M_z	Direct yaw moment
R_0	Effective radius of the tyre
T_i	Driving torque ($i = 1, 2, 3, 4$)
t_w	Wheel track width
v_x	Longitudinal velocity
v_y	Lateral velocity

1. Introduction

Electric vehicles (EVs) are an important component of a fossil-fuel-free future and the number of EVs on the roads is increasing rapidly. There are several solutions for electrified powertrains, one of which is in-wheel motor technology. In the case of 4 in-wheel motors (4IWMs), the propelling power of each wheel can be independently controlled. Therefore, 4IWM EVs can provide more control flexibility than traditional centralised driving vehicles. For example, direct yaw moment control (DYC) can easily be implemented in a 4IWM EV.

The DYC usually follows a hierarchical structure consisting of a high-level yaw moment controller and a low-level torque distribution controller. Based on a reference model, the high-level controller can determine the stability yaw moment which provides an effective way to stabilise the vehicles. Tahami et al. [1] used a fuzzy logic controller, which adopted the yaw rate error (compared to the desired yaw rate) and this yaw rate error rate of change as inputs and the torque difference between the right and left wheels as the output to generate the DYC, for the purpose of enhancing the vehicle stability. Raksincharoensak et al. [2] proposed two types of desired yaw rate: one for the lane-keeping function and the other for vehicle stability control to improve the vehicle handling and stability. A driver steering behaviour recognition algorithm, using the steering wheel angle and the steering wheel velocity as inputs, was designed to determine the type of desired yaw rate. Geng et al. [3] took, besides the desired yaw rate, the desired body slip angle into account and adopted the linear quadratic regulator method to calculate the optimal yaw moment. Thereby, the vehicle body slip angle can also be controlled with DYC. Nam et al. [4] also considered both the desired yaw rate and the body slip angle although an output feedback stability control system was used to derive the expected yaw moment. Sliding mode control (SMC) of DYC has also been studied, because of its robustness to uncertainties, finite-time convergence and reduced-order compensated dynamics [5]. Chen et al. [6] used the desired yaw rate to construct the sliding surface and Ding et al. [7] further considered both the desired yaw rate and body slip angle. Through convergence to the surface, DYC for tracking the desired signals can be derived.

Because of the limited driving range of electric vehicles, energy-efficient control is considered a very important research field. The low-level controller of the hierarchical DYC mentioned above can optimise the torque distribution to improve the energy-efficiency based on the yaw moment from the high-level controller and the total torque demand. Dizqahet et al. [8] and Lenzo et al. [9] used the hierarchical structure and studied the low-level torque distributions based on the power loss characteristics of a single drivetrain. Zhai et al. [10] optimised the wheel load usage and energy consumption in the low-level control, but motor efficiency characteristics were not considered. Some researchers in [11,12] have taken the motor efficiency characteristics into account when optimising the energy-efficient torque distribution. Energy-efficient control is achieved by the low-level controller rather than the high-level controller.

The hierarchical structure for DYC can only provide a fixed yaw moment for each time step. During cornering, for example when driving in a circle, different yaw moment and front steering angle can be combined together to keep the same path. That gives a potential to be more energy-efficient by having a yaw moment range to choose from. A DYC for energy-efficiency was proposed in previous work [13], which provided a range of direct yaw moment for low-level torque distribution controller. With the pre-known information of the motor efficiency, optimisation was carried out in the yaw moment range to find the most energy-efficient yaw moment.

The energy saving function of the DYC for energy-efficiency in [13] has been demonstrated under non-safety-critical cornering manoeuvres. The behaviour of the DYC for energy-efficiency is also analysed under safety-critical cornering manoeuvres in this work. The results show that the DYC for energy-efficiency cannot keep the vehicle safe under safety-critical cornering manoeuvres. Therefore, during cornering manoeuvres, including both non-safety-critical parts and safety-critical parts, this work proposes a combination of the DYC for energy-efficiency and a DYC for stability, which tracks the reference yaw rate, and a switching principle, alternating between the DYC for energy-efficiency and the DYC for stability, has been designed to keep the vehicle both energy-efficient and safe. This work is building on the idea first presented in [14]. Here the concept is more thoroughly investigated.

The outline of this paper is as follows. Firstly, Section 2 presents the vehicle model and driver model. Section 3 describes the offline torque distribution rule based on motor efficiency curve and the potential of DYC on energy saving during steady-state cornering. Also covered in this section are the yaw moment range and the structure of the DYC for energy-efficiency. Section 4 introduces the DYC for stability and the stability judgement. Section 5 presents the performance of equal torque driving, DYC for energy-efficiency and DYC for stability under both non-safety-critical cornering manoeuvres and safety-critical cornering manoeuvres. In Section 6, the switching principle for alternating between the DYC for energy-efficiency and the DYC for stability is designed. Section 7 shows the results of switching principle during safety-critical cornering manoeuvres. Finally, some conclusions are provided in Section 8.

2. Vehicle model and driver model

The investigated vehicle is a 4IWMs EV and the vehicle planar motion models can be seen in reference [13]. The vehicle parameters are shown in Table 1. The vehicle parameters

do not change between the different powertrain configurations and the different torque distribution methods.

Magic Formula [15] tyre models for the longitudinal and the lateral forces are used in the present study. The coefficients are derived from Appendix 3 in [15]. The equations for longitudinal and lateral forces can be seen in reference [13].

Based on the characteristics of the in-wheel motor data in [12], a simplified in-wheel motor efficiency curve is designed for the chosen vehicle, see Figure 1. Since only constant velocity cornering manoeuvres are considered in this work, the efficiency is a function of the motor torque. This motor efficiency curve is scaled up compared to the one in [12]. The torque range of each individual motor is from -200 Nm to 400 Nm. The total torque of the 4IWMs is set to 1600 Nm, which firstly allows the vehicle to be able to start from an 18% slope [16] at 0 km/h with a longitudinal acceleration of 0.7 m/s², and secondly, makes the vehicle be able to maintain a longitudinal acceleration of 2.4 m/s² at 80 km/h.

The total power loss for the vehicle is calculated as

$$P = \sum_{i=1}^4 T_i \omega_i \left(\frac{1 + \text{sign}(T_i)}{2} \frac{1}{\eta(T_i)} + \frac{1 - \text{sign}(T_i)}{2} \eta(T_i) \right) \quad (1)$$

where $\eta(T_i)$ is the motor efficiency as a function of motor torque T_i .

The driver model contains a PID controller to maintain the desired velocity and a preview steering model [17–19] to follow the desired path. The illustration of the preview steering model can be seen in reference [13].

Table 1. Vehicle parameters.

Parameter	Value	Parameter	Value	Parameter	Value	Parameter	Value
m	2062kg	l_r	1.56 m	l_f	0.97 m	l_z	2674 kgm ²
t_w	1.578 m	l_w	1 kgm ²	h	0.6 m	R_0	0.3 m
C_{ar}	0.3	A	2 m ²	f_{rr}	0.01		

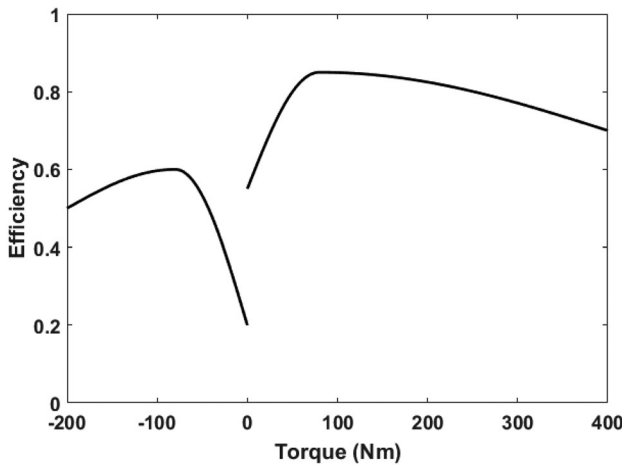


Figure 1. The designed motor efficiency curve.

3. Design of DYC for energy-efficiency

The offline torque distribution, based on the motor efficiency curve, is found by optimisation. The contribution of DYC to power loss reduction, during steady-state cornering, is studied. The yaw moment range, based on a reference lateral acceleration a_{yr} , is designed. The structure of a DYC for energy-efficiency is designed.

3.1. Offline torque distribution rule

Because the tyre's longitudinal slip ratio κ_i is usually small, it can be assumed that rotational speeds of left wheels are equal, namely $\omega_1 = \omega_3$ and $\omega_2 = \omega_4$. Left wheels' torques (T_1 and T_3) and right wheels' torques (T_2 and T_4) can be considered separately. For example, for the left wheels' torques T_1 and T_3 , the power usage of T_1 and T_3 can be expressed as P_{13} in the following equation

$$P_{13} = \left[\left(\frac{1 + \text{sign}(T_1)}{2} \frac{T_1}{\eta(T_1)} + \frac{1 - \text{sign}(T_1)}{2} T_1 \eta(T_1) \right) + \left(\frac{1 + \text{sign}(T_3)}{2} \frac{T_3}{\eta(T_3)} + \frac{1 - \text{sign}(T_3)}{2} T_3 \eta(T_3) \right) \right] \omega_1 \quad (2)$$

Since ω_1 in Equation (2) is constant at each time step, the minimisation of P_{13} can be simplified as minimisation of P_{13s} which is expressed as

$$P_{13s} = \left(\frac{1 + \text{sign}(T_1)}{2} \frac{T_1}{\eta(T_1)} + \frac{1 - \text{sign}(T_1)}{2} T_1 \eta(T_1) \right) + \left(\frac{1 + \text{sign}(T_3)}{2} \frac{T_3}{\eta(T_3)} + \frac{1 - \text{sign}(T_3)}{2} T_3 \eta(T_3) \right) \quad (3)$$

The sum of T_1 and T_3 is expressed as T_{13} (the sum of T_2 and T_4 is expressed as T_{24}) and the optimisation of the P_{13s} can be formulated as

$$\begin{array}{ll} \text{Minimise} & P_{13s} \\ \text{Constraints} & T_1 + T_3 = T_{13} \\ & T_1 \in [-200, 400] \text{Nm} \\ & T_3 \in [-200, 400] \text{Nm} \\ & T_{13} \in [-400, 800] \text{Nm} \end{array} \quad (4)$$

The resulting offline optimal distribution of T_1 and T_3 based on T_{13} for the motor efficiency curve is shown in Equation (5).

$$\begin{cases} T_1 = T_3 = T_{13}/2 & -400 \text{Nm} \leq T_{13} \leq -136 \text{Nm} \\ T_1 = 0, T_3 = T_{13} & -136 \text{Nm} < T_{13} < 142 \text{Nm} \\ T_1 = T_3 = T_{13}/2 & 142 \text{Nm} \leq T_{13} \leq 800 \text{Nm} \end{cases} \quad (5)$$

3.2. The contribution of *DYC* to power loss reduction during steady-state cornering

The yaw motion of the vehicle can be expressed as

$$I_z \ddot{\psi} = (F_{x1} \sin \delta_f + F_{x2} \sin \delta_f + F_{y1} \cos \delta_f + F_{y2} \cos \delta_f) l_f - (F_{y3} + F_{y4}) l_r \\ + (F_{x2} \cos \delta_f - F_{y2} \sin \delta_f - F_{x1} \cos \delta_f + F_{y1} \sin \delta_f + F_{x4} - F_{x3}) t_w / 2 \quad (6)$$

Since the front steering angle δ_f is usually small, the direct yaw moment M_z is defined and simplified as

$$M_z = (F_{x2} \cos \delta_f - F_{y2} \sin \delta_f - F_{x1} \cos \delta_f + F_{y1} \sin \delta_f + F_{x4} - F_{x3}) t_w / 2 \\ \approx (F_{x2} - F_{x1} + F_{x4} - F_{x3}) t_w / 2 \quad (7)$$

Total torque demand T_{all} ($T_{all} = T_1 + T_2 + T_3 + T_4$) can be derived from the M_z input which can be seen in reference [13] and T_{13} and T_{24} can be expressed as

$$T_{13} = \frac{1}{2} \left[T_{all} - M_z \frac{2R_0}{t_w} - (F_{z4} + F_{z2} - F_{z1} - F_{z3}) f_{rr} R_0 \right] \quad (8)$$

$$T_{24} = \frac{1}{2} \left[T_{all} + M_z \frac{2R_0}{t_w} + (F_{z4} + F_{z2} - F_{z1} - F_{z3}) f_{rr} R_0 \right] \quad (9)$$

The distribution of T_1 and T_3 based on T_{13} and the distribution of T_2 and T_4 based on T_{24} follow the rules in Equation (5).

By analysing the vehicle characteristics in steady-state cornering, the fundamental vehicle motion characteristics can be understood [20]. During steady-state cornering, it can be assumed that $\dot{v}_x = 0, \dot{v}_y = 0$ and $\ddot{\psi} = 0$. The case of $v_x = 80 \text{ km/h}$, $\mu = 0.8$ and $a_y \in [0.1, 4] \text{ m/s}^2$ under the yaw moment range $M_z \in [-1000, 1000] \text{ Nm}$ is firstly studied.

The results are shown in Figure 2. In Figure 2(a), it can be seen that there are two local minimal power loss P lines during the whole range of a_y , i.e. the local minimal power loss line at positive M_z and at negative M_z . For comparison, two-rear-wheel equal torque driving (2WETD) and four-wheel equal torque driving (4WETD) are also studied. In Figure 2(b), it can be seen that the two local minimal power loss lines in Figure 2(a) can reduce the power loss considerably compared to that of 4WETD and can also consume less power than that of 2WETD when $a_y < 1.6 \text{ m/s}^2$. In Figure 2(c), it is shown that at each a_y , positive M_z can reduce the total torque demand T_{all} . In Figure 2(d–e), it is shown that δ_f can be reduced by positive M_z and can be even negative when a_y is low and M_z is large (The tyre slip loss caused by negative δ_f , which is counter-steering, is not considered). From [21,22], the understeer gradient is defined in Equation (10). In Figure 2(f), the understeer gradients K_{us} of equal torque driving (2WETD and 4WETD have the same understeer gradient) and the two local minimal power loss lines are presented. The vehicle is understeered using equal torque driving. The local minimal power loss line at negative M_z can increase the K_{us} . The local minimal power loss line at positive M_z can reduce the K_{us} ; however, since $K_{us} > 0$, the vehicle is still understeered.

$$K_{us} = \frac{-\partial \left[\frac{\alpha_1 + \alpha_2}{2} - \frac{\alpha_3 + \alpha_4}{2} \right]}{\partial a_y} \quad (10)$$

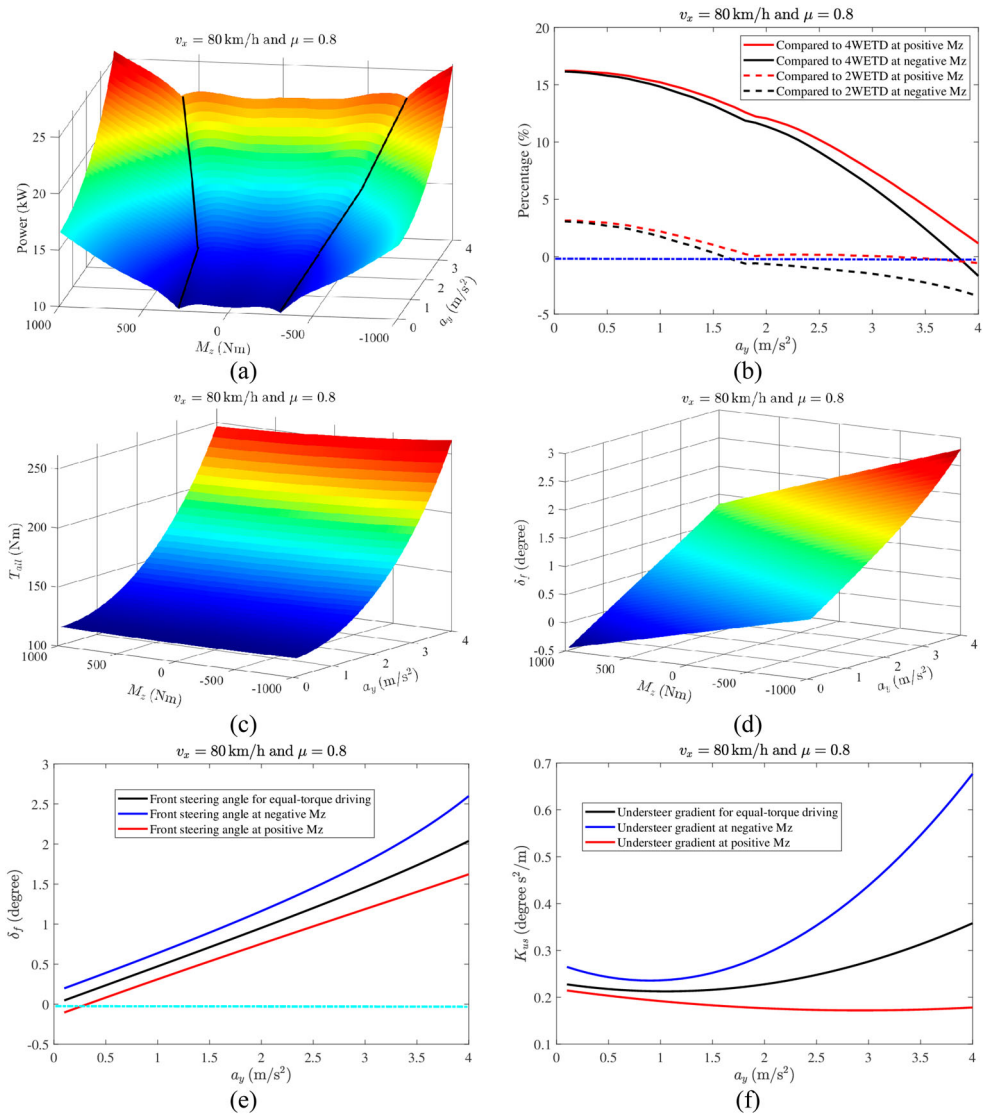


Figure 2. Results of steady-state cornering at $v_x = 80 \text{ km/h}$ and $\mu = 0.8$: (a) power loss P versus M_z and a_y ; (b) percentage of power loss reduction compared to 4WETD and 2WETD; (c) total torque demand T_{all} versus M_z and a_y ; (d) front steering angle δ_f versus M_z and a_y ; (e) δ_f for equal torque driving, local minimal power loss line at negative M_z and local minimal power loss line at positive M_z ; (f) understeer gradient K_{us} .

3.3. Yaw moment range design

In [23], Filippis et al. analysed the effect of different understeer characteristics on the power loss and found that a less understeered vehicle can reduce the power loss. A reference energy-efficient understeering behaviour was suggested for each velocity. However, from Figure 2, the most energy-efficient understeer gradient is not a constant value in this studied vehicle. Instead of proposing a reference energy-efficient understeer gradient, a yaw moment range is designed.

From Figure 2, it can be seen that the local minimal power loss line at positive M_z can consume less power than the local minimal power loss line at negative M_z . From Figure 2(f), it is shown that negative M_z can increase the $K_{\mu s}$ and the vehicle is more under-steered which can increase the turning burden. It can also be seen in Figure 2(e) that the local minimal power loss line at negative M_z can increase the δ_f . From the prospects of both power loss and understeer gradient, it is better to follow the local minimal power loss line at positive M_z . However, from Figure 2(b), the local minimal power loss line at positive M_z is not always more energy-efficient than 2WETD and from Figure 2(e), the δ_f of the local minimal power loss line at positive M_z can be negative (counter-steering) when a_y is low. Therefore, a method for designing the M_z range is proposed. This M_z range covers the local minimal power loss line at positive M_z and the M_z of equal torque driving. Besides, the constraint to avoid counter-steering is considered.

A reference lateral acceleration a_{yr} is designed in Equation (11). This a_{yr} represents the driver's intention from the bicycle model using equal torque driving.

$$a_{yr} = \frac{1}{\frac{L}{v_x^2} - \frac{l_r m}{LC_f} + \frac{l_f m}{LC_r}} \delta_f \quad (11)$$

When the a_{yr} is positive, i.e. left turn, δ_f should be bigger than that of neutral steering to avoid over steering, namely

$$\delta_f \geq \frac{L}{v_x^2} a_{yr} \quad (12)$$

From Figure 2(d,e), it is shown that δ_f can be influenced by M_z . Using the bicycle model and a linear tyre force model, δ_f can be expressed as a function of a_y and the direct yaw moment M_z under steady-state cornering [24] which is shown as

$$\delta_f = \left(\frac{L}{v_x^2} - \frac{l_r m}{LC_f} + \frac{l_f m}{LC_r} \right) a_y + \left(\frac{1}{LC_f} + \frac{1}{LC_r} \right) M_z \quad (13)$$

When a_{yr} is positive and δ_f is needed to be $\geq \frac{L}{v_x^2} a_{yr}$ shown in Equation (12), one side of the M_z range derived from Equation (13) can be expressed as

$$M_z \leq - \left(-\frac{l_r m}{LC_f} + \frac{l_f m}{LC_r} \right) a_{yr} / \left(\frac{1}{LC_f} + \frac{1}{LC_r} \right) \quad (14)$$

The other side of the M_z range is not less than the yaw moment of the equal-torque driving, i.e.

$$M_z \geq (F_{x4e} + F_{x2e} - F_{x1e} - F_{x3e})t_w/2 \quad (15)$$

where

$$F_{xie} = (T_{all}/4 - F_{zi}f_{rr}R_0)/R_0 \quad (16)$$

When a_{yr} is negative, i.e. a right turn, the design of M_z follows the same rule of when a_{yr} is positive.

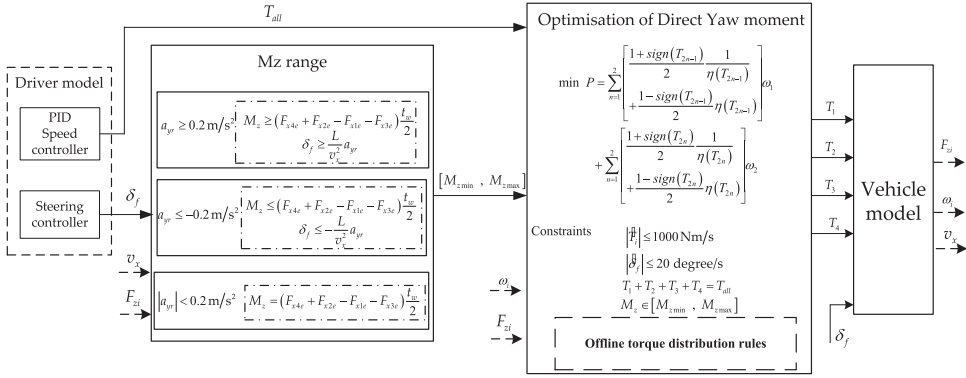


Figure 3. The controller structure of the DYC for energy-efficiency.

During straight driving or during change in vehicle's direction, a_{yr} can be equal to zero and the direct yaw moment M_z follows the value in Equation (17).

$$M_z = (F_{x4e} + F_{x2e} - F_{x1e} - F_{x3e})t_w/2 \quad (17)$$

The yaw moment range designs for $a_{yr} > 0$, $a_{yr} < 0$ and $a_{yr} = 0$ can be summarised as

$$\begin{cases} M_z \in \left[M_{ze}, -\left(-\frac{l_r m}{LC_f} + \frac{l_f m}{LC_r}\right) a_{yr} / \left(\frac{1}{LC_f} + \frac{1}{LC_r}\right) \right] & (a_{yr} > 0) \\ M_z \in \left[-\left(-\frac{l_r m}{LC_f} + \frac{l_f m}{LC_r}\right) a_{yr} / \left(\frac{1}{LC_f} + \frac{1}{LC_r}\right), M_{ze} \right] & (a_{yr} < 0) \\ M_z = (F_{x4e} + F_{x2e} - F_{x1e} - F_{x3e})t_w/2 & (a_{yr} = 0) \end{cases} \quad (18)$$

where $M_{ze} = (F_{x4e} + F_{x2e} - F_{x1e} - F_{x3e})t_w/2$.

3.4. The controller structure design of DYC for energy-efficiency

The controller structure of DYC for energy-efficiency is designed and can be seen in Figure 3. The PID speed controller can output the total torque demand T_{all} to follow the reference velocity. The steering controller can output the front steering angle command δ_f . The yaw moment range $[M_{z\min}, M_{z\max}]$ is calculated using the method presented in Section 3.3 and only when $|a_{yr}| \geq 0.2\text{m/s}^2$, the DYC for energy-efficiency is active. With each $M_z \in [M_{z\min}, M_{z\max}]$ and T_{all} , T_{13} and T_{24} are calculated based on Equations (8) and (9) and the distribution of T_1 , T_2 , T_3 and T_4 follows the rules in Equation (5). In the M_z range $[M_{z\min}, M_{z\max}]$, the Golden Section Search method is used to search for the most energy-efficient M_z to reach the minimal power consumption. The rate of change for T_i and δ_f is limited as

$$\begin{cases} |\dot{T}_i| \leq 1000\text{Nm/s} \\ |\dot{\delta}_f| \leq 20\text{degree/s} \end{cases} \quad (19)$$

4. DYC for stability and stability judgement

4.1. Stability DYC

In this study, the function of the designed DYC for stability is to track the reference yaw rate $\dot{\psi}_r$ and the sliding mode control (SMC) method is used. From [20], $\dot{\psi}_r$ is calculated as

$$\dot{\psi}_r = \frac{v_x}{L + \frac{mv_x^2}{L} \left(\frac{l_f}{C_r} - \frac{l_r}{C_f} \right)} \delta_f \quad (20)$$

The designed sliding surface is expressed as

$$e = \psi - \dot{\psi}_r + k_1 \int (\dot{\psi} - \dot{\psi}_r) dt \quad (21)$$

where k_1 is a coefficient. The reaching law of the SMC is designed to be

$$\dot{e} + k_2 \text{sign}(e) = 0 \quad (22)$$

where $k_2 > 0$. Then the stability yaw moment M_{zs} can be expressed as

$$M_{zs} = I_z(\ddot{\psi}_r - k_1(\dot{\psi} - \dot{\psi}_r) - k_2 \text{sign}(e)) - (F_{y12}l_f - F_{y34}l_r) \quad (23)$$

where F_{y12} and F_{y34} are the lateral forces for front and rear tyres, respectively.

$$F_{y12} = C_f(\beta + l_f\dot{\psi}/v_x - \delta_f) \quad (24)$$

$$F_{y34} = C_r(\beta - l_r\dot{\psi}/v_x) \quad (25)$$

4.2. Stability judgement

The vehicle stability working area can be a combination of the yaw rate $\dot{\psi}$ and the body slip angle β . In Rajamani [25], the suggested simplified ranges for yaw rate and body slip angle are

$$\begin{cases} |\dot{\psi}| \leq 0.85 \frac{\mu g}{v_x} \\ |\beta| \leq \text{atan}(0.02\mu g) \end{cases} \quad (26)$$

Given different initial $\dot{\psi}$ and β , the $\dot{\psi} - \beta$ phase-plane method [26–28] can divide the vehicle working area into a stability region and a non-stability region. According to the mathematical analysis, the Lyapunov method [29,30] can also give a theoretical $\dot{\psi} - \beta$ stability region.

In Figure 4, these three stability region methods (phase-plane, Lyapunov and simplified ranges) are compared for two cases: $v_x = 50\text{km/h}$ and $\mu = 0.35$, and $v_x = 80\text{km/h}$ and $\mu = 0.8$. The steering angle for the phase-plane method as well as the Lyapunov method is zero. It can be observed in Figure 4(a) and (b) that the simplified ranges in Equation (26) are within the phase-plane stability area and that the Lyapunov method results in large body slip angles and yaw rates. Therefore, the simplified range described by Equation (26) is chosen for stability judgement in the present study.

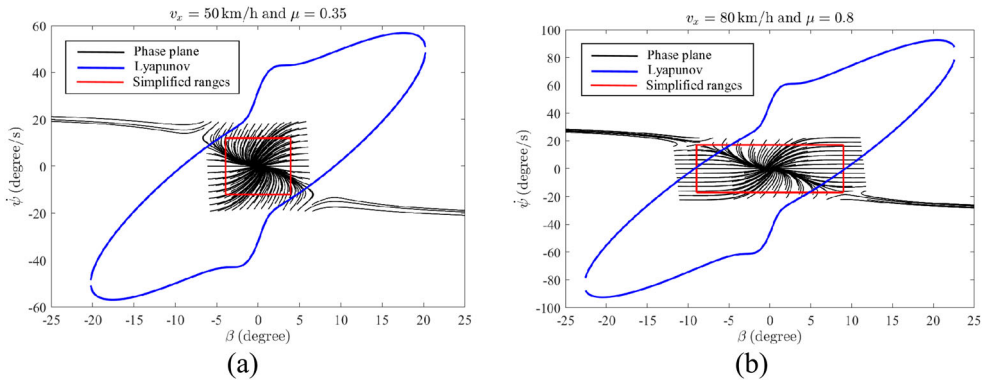


Figure 4. Comparison of stability regions: (a) $v_x = 50 \text{ km/h}$ and $\mu = 0.35$; (b) $v_x = 80 \text{ km/h}$ and $\mu = 0.8$.

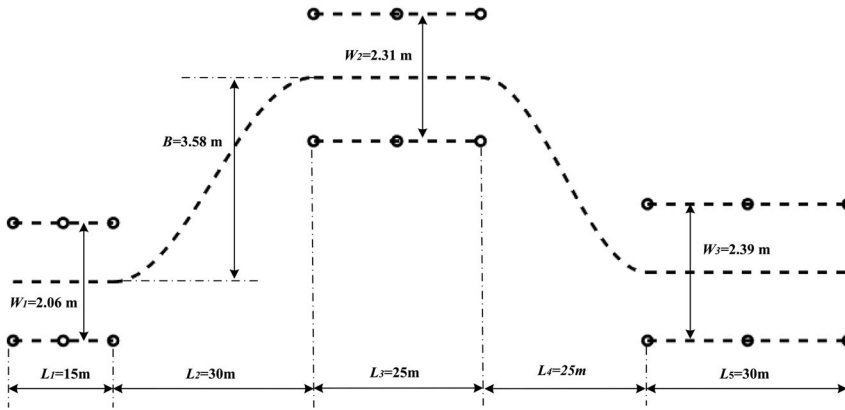


Figure 5. Description of the studied double lane change manoeuvre.

5. Performance of the DYC for energy-efficiency and the DYC for stability

To verify the effectiveness of the controller during continuous driving, simulations are carried out using the ISO 3888-1 double lane change manoeuvre [31], which is illustrated in Figure 5. The path parameters of ISO 3888-1 double lane change are also shown in Figure 5. In addition, an extended double lane change for light manoeuvres is designed with $L_2 = 60 \text{ m}$ and $L_4 = 50 \text{ m}$ and other parameters are the same with those of ISO 3888-1 in Figure 5. The vehicle will take the dotted line in Figure 5 as reference path. The illustration of the dotted line can be seen in reference [13].

Firstly, the EV's behaviour and energy consumption, in the extended double lane change with $v_x = 50 \text{ km/h}$ and $\mu = 0.35$ and extended double lane change with $v_x = 80 \text{ km/h}$ and $\mu = 0.8$, are analysed. These two cornering manoeuvres are light and non-safety-critical. Secondly, the ISO 3888-1 double lane change with $v_x = 50 \text{ km/h}$ and $\mu = 0.35$ and the ISO 3888-1 double lane change with $v_x = 80 \text{ km/h}$ and $\mu = 0.8$ are studied. These two manoeuvres are severe and contain both non-safety-critical cornering and safety-critical

Table 2. Average power consumption and the percentage reduction for the simulated driving tests.

			Average power (kW)	Reduction (%)
$v_x = 50\text{km/h}$ $\mu = 0.35$	Extended	4WETD	5.77	15.42
		2WETD	5.04	3.17
		DYC for energy-efficiency	4.88	
		DYC for stability	5.22	6.51
$v_x = 80\text{km/h}$ $\mu = 0.8$	Extended	4WETD	11.84	14.52
		2WETD	10.27	1.46
		DYC for energy-efficiency	10.12	
		DYC for stability	12.15	16.7
$v_x = 50\text{km/h}$ $\mu = 0.35$	ISO 3888-1	4WETD	unsafe	
		2WETD	unsafe	
		DYC for energy-efficiency	unsafe	
		DYC for stability	6.8	12.5
		Combined DYC	5.95	
$v_x = 80\text{km/h}$ $\mu = 0.8$	ISO 3888-1	4WETD	unsafe	
		2WETD	unsafe	
		DYC for energy-efficiency	unsafe	
		DYC for stability	20.62	18.8
		Combined DYC	16.73	

cornering. For low friction $\mu = 0.35$, $C_f = -42.7\text{kN/rad}$ and $C_r = -36.7\text{kN/rad}$. For high friction $\mu = 0.8$, $C_f = -97.6\text{ kN/rad}$ and $C_r = -84\text{ kN/rad}$.

Four torque distribution methods are used, i.e. 4WETD, 2WETD, DYC for energy-efficiency and DYC for stability. Except average power consumption, 4WETD shows the same behaviour as 2WETD. Therefore, 4WETD results are not plotted and average power consumptions of 4WETD are discussed. The average power consumption and the percentage reduction in the power consumption for all the simulated manoeuvres are listed in Table 2.

5.1. Non-safety-critical manoeuvres

5.1.1. Extended double lane change with $v_x = 50\text{ km/h}$ and $\mu = 0.35$

This sub-section deals with the extended double lane change with a low road friction $\mu = 0.35$ and a longitudinal velocity of 50 km/h, whose simulation results are shown in Figure 6. From Figure 6(a,b), it is shown that 2WETD, DYC for energy-efficiency and DYC for stability follow the same path and the same velocity. In Figure 6(a), the middle lines are trajectories of CoG and the outerlines are trajectories of the vehicle's four corners. From Figure 6(c), it is seen that 2WETD, DYC for energy-efficiency and DYC for stability are all safe during this manoeuvre and DYC for stability has the smallest stability working area. From Figure 6(d), it is seen that DYC for energy-efficiency consumes less power and DYC for stability can consume more power than 2WETD. The average power consumption of 4WETD is 5.77 kW, that of 2WETD is 5.04 kW, that of DYC for energy-efficiency is 4.88 kW and that of DYC for stability 5.22 kW. The DYC for energy-efficiency can save 15.42% energy compared to 4WETD, 3.17% compared to 2WETD and 6.51% compared to DYC for stability. The torque distributions of the four wheels are shown in Figure 6(e). The yaw moments M_z are shown in Figure 6(f). The steering angles δ_f are shown in Figure 6(g)

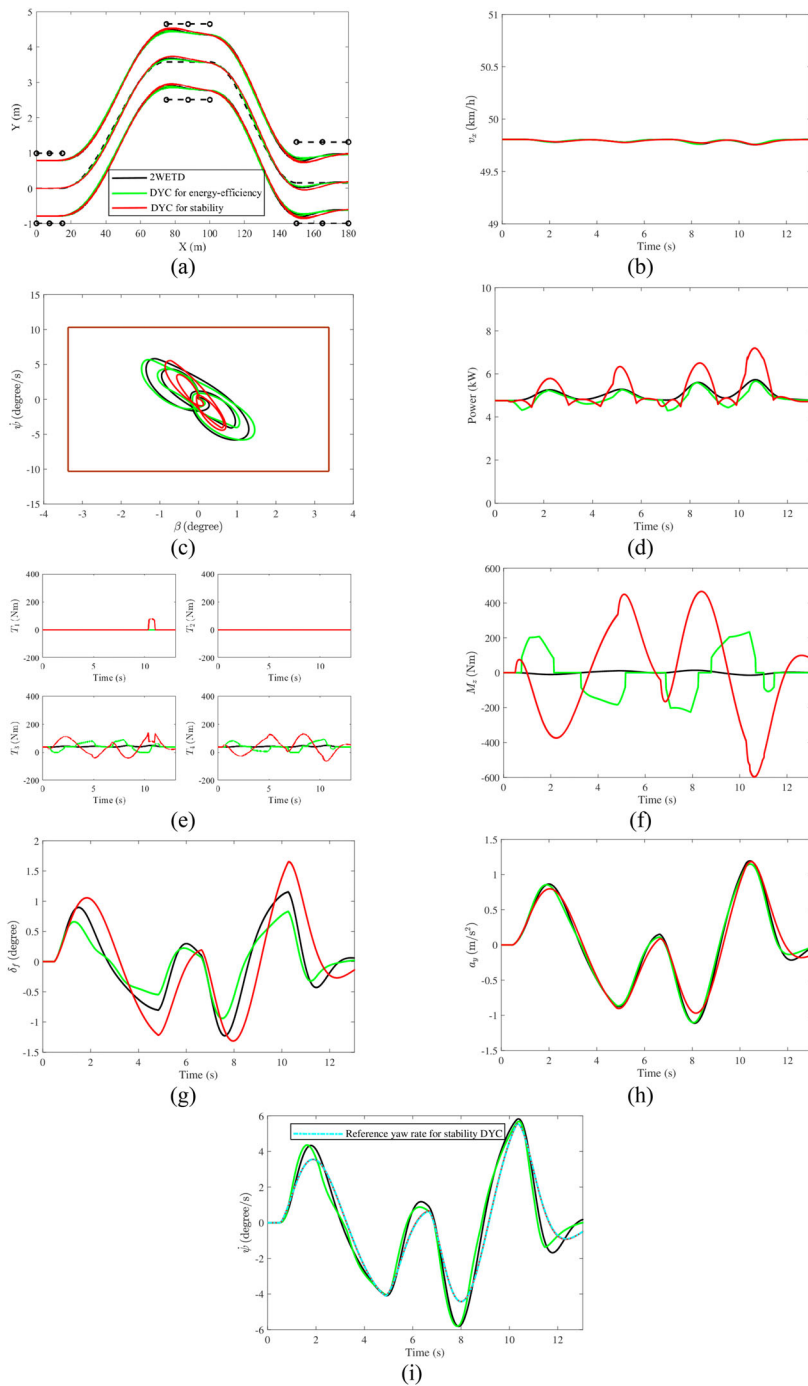


Figure 6. Results for extended double lane change with $v_x = 50$ km/h and $\mu = 0.35$: (a) path; (b) longitudinal velocity; (c) stability working area; (d) power; (e) wheel torques; (f) yaw moment; (g) front steering angle; (h) lateral acceleration; (i) yaw rate.

and these three torque distribution methods all have continuous steering angles. The lateral accelerations a_y are shown in Figure 6(h). From Figure 6(i), it is shown that DYC for stability can reduce the yaw rate $\dot{\psi}$ and can closely track the reference yaw rate $\dot{\psi}_r$.

5.1.2. Extended double lane change with $v_x = 80$ km/h and $\mu = 0.8$

The simulation results for $v_x = 80$ km/h and $\mu = 0.8$ during the extended double lane change manoeuvre are shown in Figure 7. In Figure 7(c), it is shown that the working areas are within the stability region, so that this is a light manoeuvre. The DYC for stability also shows smaller working area than the other two methods. In Figure 7(d), it is shown that DYC for energy-efficiency has the lowest power consumption. The average power loss of 4WETD is 11.84 kW, that of 2WETD is 10.27 kW, that of DYC for energy-efficiency is 10.12 kW and that of DYC for stability is 12.15 kW. The DYC for energy-efficiency can save 14.52% energy compared to 4WETD, 1.46% compared to 2WETD and 16.7% compared to DYC for stability. From Figure 7(i), it is also shown that the DYC for stability can reduce the yaw rate $\dot{\psi}$ and closely track the reference yaw rate $\dot{\psi}_r$.

5.2. Safety-critical manoeuvres

The stability working area of $v_x = 50$ km/h and $\mu = 0.35$ during the ISO 3888–1 double lane change is shown in Figure 8(a). The working area of $v_x = 80$ km/h and $\mu = 0.8$ under ISO 3888–1 double lane change is shown in Figure 8(b). It is seen that these are two severe manoeuvres, i.e. DYC for energy-efficiency and 2WETD cannot keep the vehicle in the safety region. However, it is seen that only DYC for stability can keep the vehicle within the safety region, as defined in Equation (26).

6. Switching principle

From Figure 8, it is shown that only the DYC for stability can keep the vehicle within the safety region. However, from Figure 6 and Figure 7(d), it can be concluded that DYC for energy-efficiency can save considerable energy during light manoeuvres. There is a potential for both energy saving and stability if DYC for energy-efficiency and DYC for stability can be combined together during cornering manoeuvres, containing both non-safety-critical parts and safety-critical parts. A switching principle for alternating between DYC for energy-efficiency and DYC for stability is, therefore, designed. When safety-critical cornering manoeuvres are detected, the DYC for stability becomes active.

In this study, the switching principle is designed as follows: when the absolute value of any $\dot{\psi}$ or β is larger than 0.65 times the maximum allowed value in Equation (26), DYC for stability takes charge and to avoid frequent changing, the DYC for energy-efficiency is enabled again when the absolute values of both $\dot{\psi}$ and β are smaller than 0.55 times each maximum value. The switching principle is illustrated in Figure 9(a), which shows that when $s = 0$, DYC for energy-efficiency is used and when $s = 1$, DYC for stability is activated. With the designed switching principle, the proposed controller structure, of combining DYC for energy-efficiency and DYC for stability under severe manoeuvres, can be seen in Figure 9(b). The combination of DYC for energy-efficiency and DYC for stability is hereafter referred to as combined DYC.

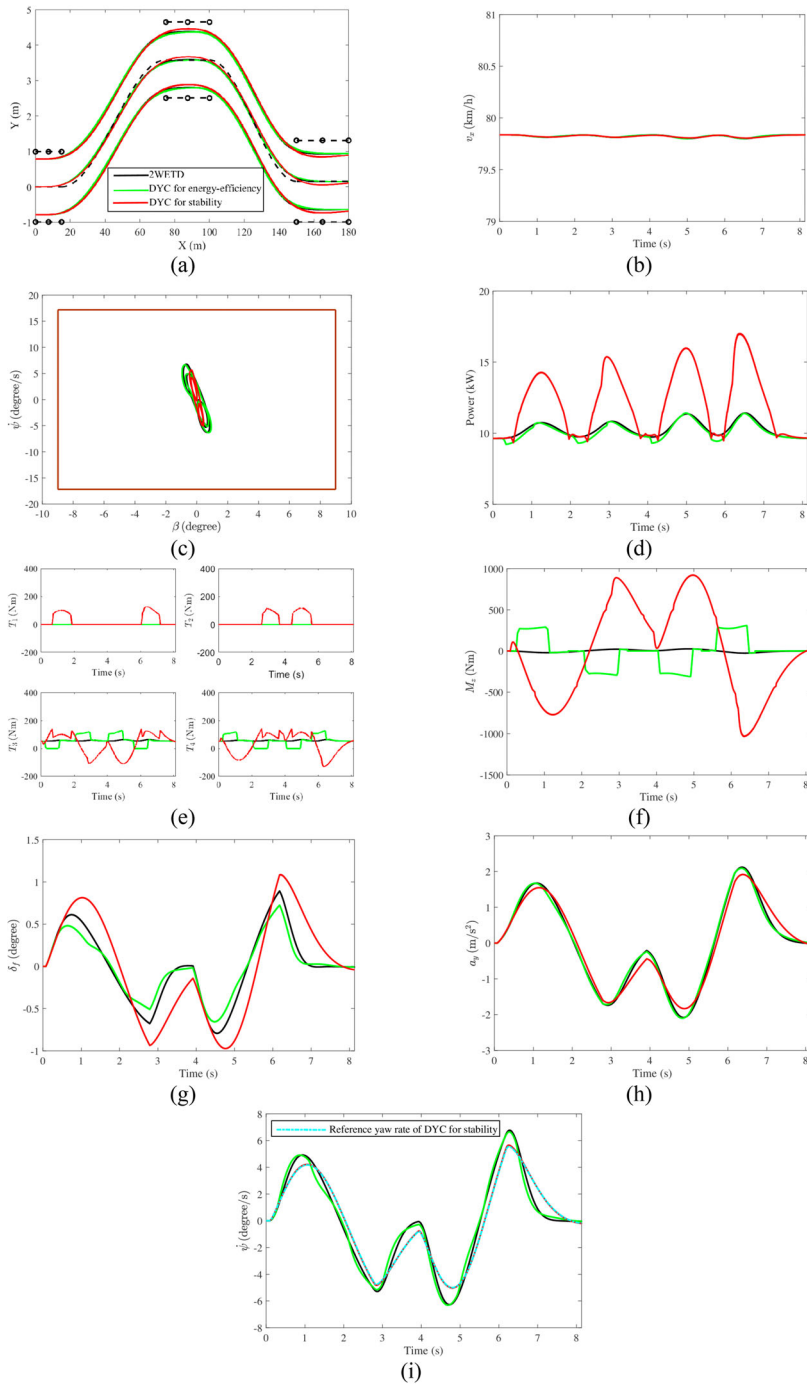


Figure 7. Results for extended double lane change with $v_x = 80$ km/h and $\mu = 0.8$: (a) path; (b) longitudinal velocity; (c) stability working area; (d) power; (e) wheel torques; (f) yaw moment; (g) front steering angle; (h) lateral acceleration; (i) yaw rate.

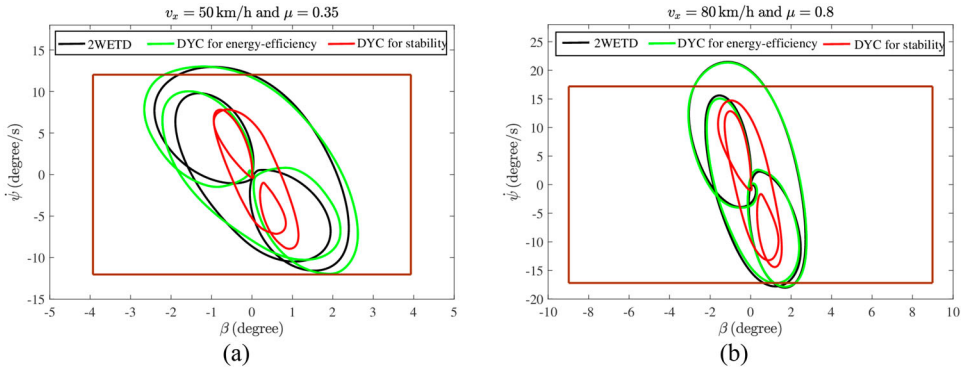


Figure 8. Stability working area for ISO 3888–1 double lane change: (a) $v_x = 50$ km/h and $\mu = 0.35$; (b) $v_x = 80$ km/h and $\mu = 0.8$.

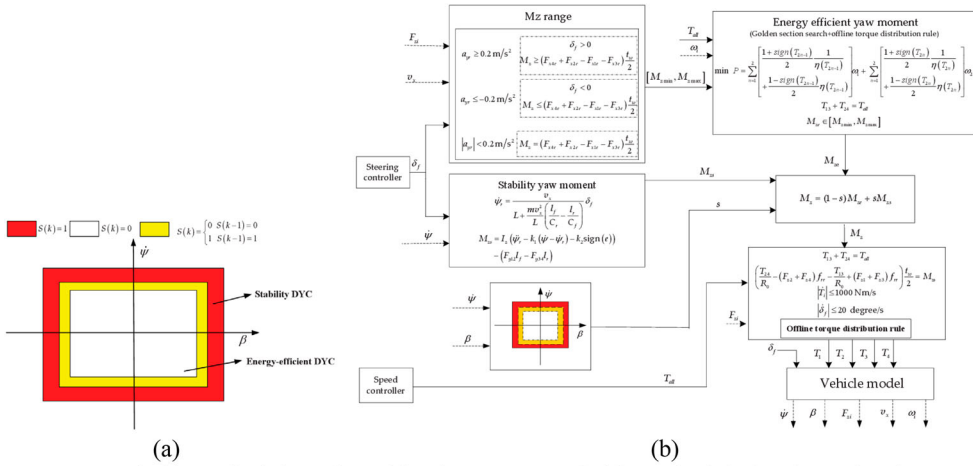


Figure 9. Switching principle and combined DYC: (a) Switching principle for alternating between DYC for energy-efficiency and DYC for stability, (b) the proposed controller structure for combination of DYC for energy-efficiency and DYC for stability: combined DYC.

7. Results of combining DYC for energy-efficiency and DYC for stability

Severe manoeuvres, $v_x = 50$ km/h and $\mu = 0.35$ under ISO 3888–1 double lane change and $v_x = 80$ km/h and $\mu = 0.8$ under ISO 3888–1 double lane change, are analysed under combined DYC and the DYC for stability.

7.1. ISO 3888–1 double lane change with $v_x = 50$ km/h and $\mu = 0.35$

The results for the ISO 3888–1 double lane change with $v_x = 50$ km/h and $\mu = 0.35$ are shown in Figure 10. In Figure 10(a,b), it is shown that the combined DYC and the DYC for stability can follow the same path and same velocity. The front steering angle δ_f is shown in Figure 10(c). In Figure 10(d), it is shown that combined DYC is able to keep the vehicle in the stability area of Equation (26). The lateral acceleration a_y is shown in Figure 10(e). In Figure 10(f), when $s = 0$, DYC for energy-efficiency is active, and when $s = 1$, DYC for

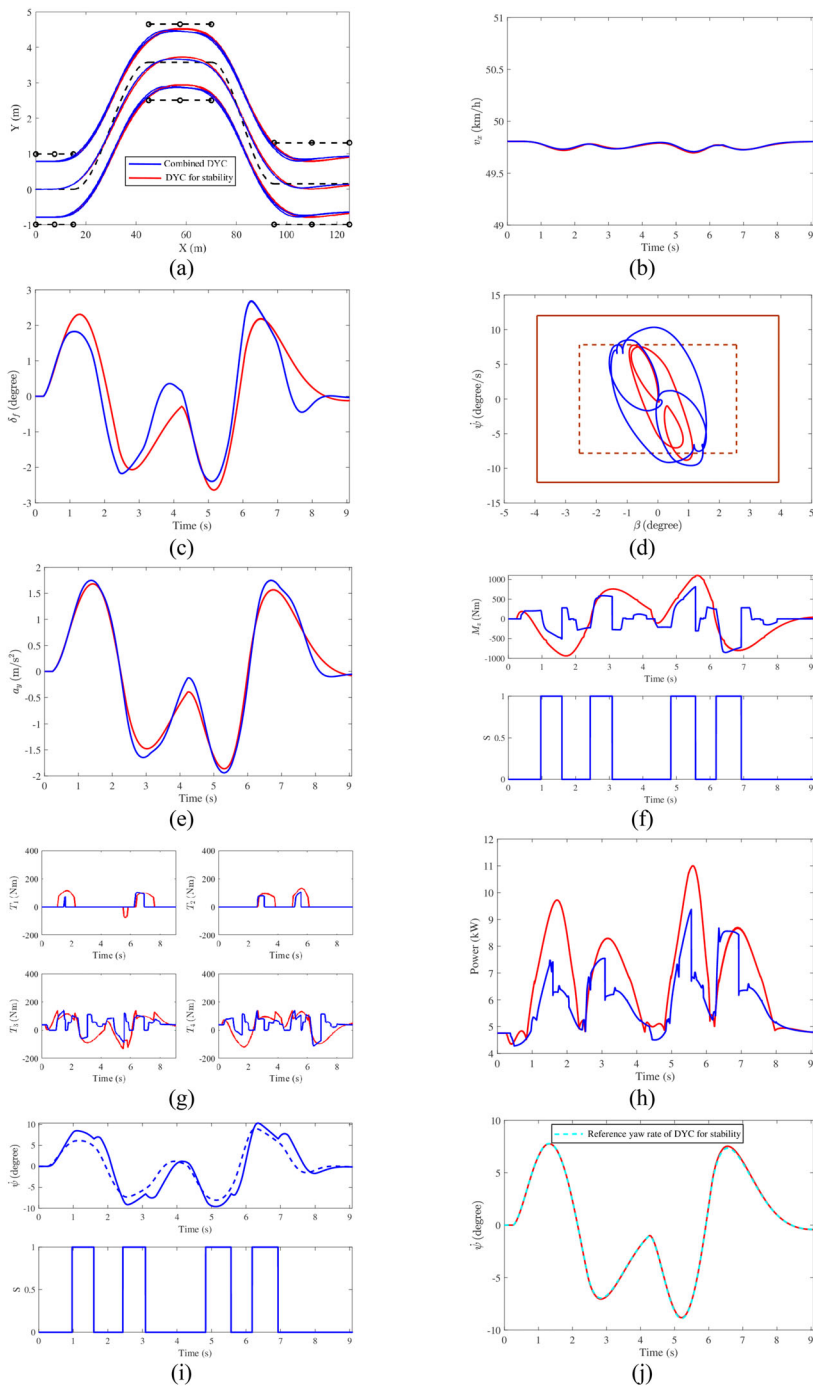


Figure 10. Results for ISO 3888–1 double lane change with $v_x = 50 \text{ km/h}$ and $\mu = 0.35$ using DYC for stability and combined DYC: (a) path; (b) longitudinal velocity; (c) front steering angle; (d) working area; (e) lateral acceleration; (f) yaw moment and S; (g) wheel torques; (h) power; (i) yaw rate of combined DYC and S; (j) yaw rate of stability DYC.

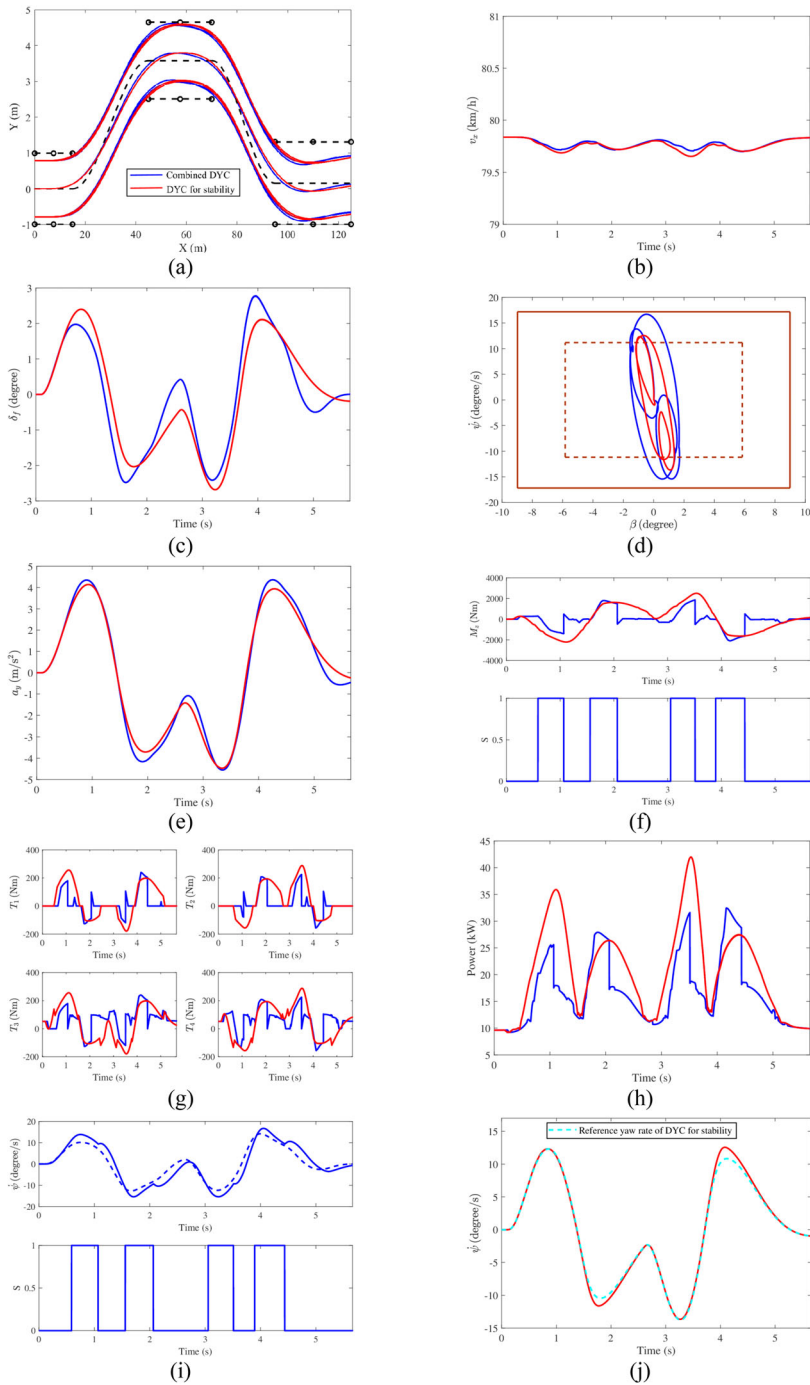


Figure 11. Results for ISO 3888–1 double lane change with $v_x = 80\text{km/h}$ and $\mu = 0.8$ using DYC for stability and combined DYC: (a) path; (b) longitudinal velocity; (c) front steering angle; (d) working area; (e) lateral acceleration; (f) yaw moment and S; (g) wheel torques; (h) power; (i) yaw rate of combined DYC and S; (j) yaw rate of stability DYC.

stability is active. The four wheels' torque distributions are shown in Figure 10(g). The power losses are shown in Figure 10(h) and it is shown that the combined DYC consumes less energy than DYC for stability. The average power loss of DYC for stability is 6.8 kW and that of combined DYC is 5.95 kW. The combined DYC can save 12.5% energy compared to DYC for stability. The yaw rate $\dot{\psi}$ change of combined DYC is shown in Figure 10(i) and it is generally shown that when the $s = 1$, the yaw rate $\dot{\psi}$ follows the trend of $\dot{\psi}_r$. The yaw rate $\dot{\psi}$ change of DYC for stability is shown in Figure 10(j) and the DYC for stability can follow the $\dot{\psi}_r$.

7.2. ISO 3888-1 double lane change with $v_x = 80$ km/h and $\mu = 0.8$

The simulation results for $v_x = 80$ km/h and $\mu = 0.8$ during the ISO 3888-1 double lane change using combined DYC are shown in Figure 11. From Figure 11(d), it can be seen that the combined DYC can keep the vehicle working within the safety boundaries. The average power loss of DYC for stability is 20.62 kW and that of combined DYC is 16.73 kW. The combined DYC can save 18.8% energy compared to DYC for stability. The yaw rate $\dot{\psi}$ change of combined DYC is shown in Figure 11(i) and it is generally shown that when the $s = 1$, the $\dot{\psi}$ follows the trend of $\dot{\psi}_r$. In Figure 11(j), although there are small deviations, it is shown that the DYC for stability can follow the trend of the $\dot{\psi}_r$.

8. Conclusion

A DYC for energy-efficiency based on the desired lateral acceleration is designed for non-safety-critical cornering manoeuvres. A DYC for stability tracking the desired yaw rate is designed for safety-critical cornering manoeuvres. In order to improve the energy efficiency and keep the vehicle safe during cornering manoeuvres which contain both non-safety-critical parts and safety-critical parts, a DYC is proposed which combines DYC for energy-efficiency and DYC for stability, which has been evaluated by simulations. A stability judgement, consisting of the yaw rate and body slip angle, is suggested and a switching principle for alternating between DYC for energy-efficiency and DYC for stability has been developed.

The following five driving strategies have been analysed: 4WETD, 2WETD, DYC for energy-efficiency, DYC for stability and combined DYC. During non-safety-critical cornering manoeuvres, the DYC for energy-efficiency can make a considerable percentage of energy saving compared to 4WETD, 2WETD and DYC for stability. It has been shown that during cornering manoeuvres containing both non-safety-critical parts and safety-critical parts, only the DYC for stability and combined DYC can keep the vehicle safe and besides the combined DYC consumes less energy than the DYC for stability.

The only online optimisation procedure in the structure is to optimise the yaw moment from the range ($M_{z \min}$, $M_{z \max}$). This optimisation is a one-dimensional search and does not need enormous calculation. Therefore, the method proposed in this study is promising for real-time implementation.

In future work it would be of interest to evaluate acceleration and deceleration as well as studying motor efficiency characteristics covering the complete speed range. Battery efficiency can be included in the whole controller structure. The switching principle, for alternating between DYC for energy-efficiency and DYC for stability, can also be explored

further to achieve smooth and comfortable vehicle behaviour. To verify the results, field tests are planned.

Disclosure statement

No potential conflict of interest was reported by the authors.

Funding

The authors greatly appreciate the support from China Scholarship Council, the Center of ECO2 Vehicle Design at KTH funded by the Swedish Innovation Agency Vinnova and the strategic research area TRENop [grant number 2016-05195].

ORCID

Peikun Sun  <http://orcid.org/0000-0002-2592-917X>

Lars Drugge  <http://orcid.org/0000-0001-8928-0368>

References

- [1] Tahami F, Farhangi S, Kazemi R. A fuzzy logic direct yaw-moment control system for all-wheel-drive electric vehicles. *Veh Syst Dyn*. Jan 2004;41(3):203–221.
- [2] Raksincharoensak P, Mizushima T, Nagai M. Direct yaw moment control system based on driver behaviour recognition. *Veh Syst Dyn*. Sep 2008;46(sup1):911–921.
- [3] Geng C, Mostefai L, Denai M, et al. Direct yaw-moment control of an in-wheel motored electric vehicle based on body slip angle fuzzy observer. *IEEE Trans Ind Electron*. May 2009;56(5):1411–1419.
- [4] Nam K, Fujimoto H, Hori Y. Lateral stability control of in-wheel-motor-driven electric vehicles based on sideslip angle estimation using lateral tire force sensors. *IEEE Trans Veh Technol*. Jun 2012;61(5):1972–1985.
- [5] Shtessel Y, Edwards C, Fridman L, et al. *Sliding mode control and observation*. New York: Springer; 2014.
- [6] Chen Y, Hedrick JK, Guo K. A novel direct yaw moment controller for in-wheel motor electric vehicles. *Veh Syst Dyn*. Jun 2013;51(6):925–942.
- [7] Ding S, Liu L, Zheng WX. Sliding mode direct yaw-moment control design for in-wheel electric vehicles. *IEEE Trans Ind Electron*. Aug 2017;64(8):6752–6762.
- [8] Dizqah AM, Lenzo B, Sornioti A, et al. A fast and parametric torque distribution strategy for four-wheel-drive energy-efficient electric vehicles. *IEEE Trans Ind Electron*. Jul 2016;63(7):4367–4376.
- [9] Lenzo B, Filippis GD, Dizqah AM, et al. Torque distribution strategies for energy-efficient electric vehicles with multiple drivetrains. *J Dyn Syst Meas Control*. Dec 2017;139(12):121004.
- [10] Zhai L, Hou R, Sun T, et al. Continuous steering stability control based on an energy-saving torque distribution algorithm for a four in-wheel-motor independent-drive electric vehicle. *Energies*. Feb 2018;11(2):350.
- [11] Han Z, Xu N, Chen H, et al. Energy-efficient control of electric vehicles based on linear quadratic regulator and phase plane analysis. *Appl Energy*. Mar 2018;213:639–657.
- [12] Chen Y, Wang J. Adaptive energy-efficient control allocation for planar motion control of over-actuated electric ground vehicles. *IEEE Trans Control Syst Technol*. Jul 2014;22(4):1362–1373.
- [13] Sun P, Stensson Trigell A, Drugge L, et al. Energy-efficient direct yaw moment control for in-wheel motor electric vehicles utilising motor efficiency maps. *Energies*. Jan 2020;13(3):593.
- [14] Sun P, Stensson Trigell A, Drugge L, et al. “Evaluation of combined energy-efficient and stability strategies utilising direct yaw moment control,” *Proceedings of the 26th IAVSD International Symposium on Dynamics of Vehicles on Roads and Tracks (IAVSD 2019)*, 12–16 August 2019, Gothenburg, Sweden.

- [15] Pacejka H. Tire and vehicle dynamics. 3rd ed. Amsterdam: Elsevier; 2012.
- [16] Giancarlo Genta LM. The automotive chassis. Dordrecht: Springer; 2008.
- [17] Symonds P, Sharp R, Casanova D. A mathematical model for driver steering control, with design, tuning and performance results. *Veh Syst Dyn*. May 2000;33(5):289–326.
- [18] Schnelle S, Wang J, Su H, et al. A driver steering model with personalized desired path generation. *IEEE Trans Syst Man Cybern Syst*. Jan 2017;47(1):111–120.
- [19] Jalali K, Lambert S, McPhee J. Development of a path-following and a speed control driver model for an electric vehicle. *SAE Int J Passeng Cars-Electron Electr Syst*. Apr 2012;5(1):100–113.
- [20] Abe M. Vehicle handling dynamics: theory and application. 2nd ed. Amsterdam: Butterworth-Heinemann; 2015.
- [21] Bucchi F, Frendo F. A new formulation of the understeer coefficient to relate yaw torque and vehicle handling. *Veh Syst Dyn*. Apr 2016;54(6):831–847.
- [22] Pacejka H. Simplified analysis of steady-state turning behaviour of motor vehicles. Part 1. Handling diagrams of simple systems. *Veh Syst Dyn*. Nov 1973;2(3):161–172.
- [23] Filippis GD, Lenzo B, Sorniotti A, et al. Energy-efficient torque-vectoring control of electric vehicles with multiple drivetrains. *IEEE Trans Veh Technol*. Jun 2018;67(6):4702–4715.
- [24] Kobayashi T, Katsuyama E, Sugiura H, et al. Direct yaw moment control and power consumption of in-wheel motor vehicle in steady-state turning. *Veh Syst Dyn*. Nov 2016;55(1):104–120.
- [25] Rajamani R. Vehicle dynamics and control. 2nd ed. Boston: Springer US; 2012.
- [26] Bobier CG, Gerdes JC. Staying within the nullcline boundary for vehicle envelope control using a sliding surface. *Veh Syst Dyn*. Feb 2013;51(2):199–217.
- [27] Ono E, Hosoe S, Tuan HD, et al. Bifurcation in vehicle dynamics and robust front wheel steering control. *IEEE Trans Control Syst Technol*. May 1998;6(3):412–420.
- [28] Pacejka HB. Non-linearities in road vehicle dynamics. *Veh Syst Dyn*. Jan 1986;15(5):237–254.
- [29] Samsundar J, Huston JC. “Estimating lateral stability region of a nonlinear 2 degree-of-freedom vehicle,” In *SAE Technical Paper Series*. SAE International, Feb 1998.
- [30] Yin G, Jin X, Qing Z, et al. Lateral stability region conservativeness estimation and torque distribution for FWIA electric vehicle steering. *Sci China Technol Sci*. Oct 2014;58(4):669–676.
- [31] Passenger Cars-Test track for a severe lane-change manoeuvre: Part 1: double lane-change. International Standards Organization (ISO) Std; 2018.